Nuclear biophysical changes during human melanoma plasticity

Maria Chiara Lionetti[a,b], Maria Rita Fumagallii[a], Caterina A. M. La Porta[a,b]

[a] *Center for Complexity and Biosystems, Department of Environmental Science and Policy, University of Milan, via Celoria 26, 20133 Milano, Italy*

[b] *CNR - Consiglio Nazionale delle Ricerche, Biophysics institute, Via De Marini 6, 16149, Genova, Italy*

Abstract

Tumor plasticity is an emerging property of tumor cells which allows them to change their phenotype in dependence on the environment. The epithelial-mesenchymal transition plays a crucial role in helping cells to acquire a more aggressive phenotype when they are in the mesenchymal state. Herein we investigated the biophysical changes occurring during phenotypic switching in human melanoma cells considering the blebbines of the nuclei, their stiffness and the involvement of polycombs with lamins. We show that the formation of cellular heterogeneity involves many crucial nuclear changes including the interaction between different types of polycombs with lamins and chromosome accessibility. All together our results shed new light on the molecular mechanisms involved in the formation of an heterogeneous cell population during phenotypic switching.

1. Introduction

Human melanoma is a rare highly resistant tumor which is accountable for almost 2% of all cancer deaths worldwide. Chemoresistance is the major issue for melanoma, contributing to poor prognosis and low survival rate of treated patients, especially when metastatic. The heterogeneity of the tumor and the presence of cancer stem cells (CSCs) plays a critical role in resistance. In fact, CSCs have not only a slow proliferative rate but also express drug efflux transporters such as ABCG2 [1]. Furthermore, more recently, it was clearly demonstrated that tumor cells, including melanoma, can change their phenotype in dependence on the environment, switching from epitelial to mesenchymal state and therefore acquiring a more aggressive phenotype [2, 3, 4, 5].

Our group recently showed that a complex network of miRNAs is differentially expressed during the phenotypic switching, driving the epithelial to mesenchymal transition (EMT) [4]. Among these miRNAs, there is hsa-mir-222 whose role on phenotypic switching was further investigated more recently [3]. It was shown that hsa-mir-222 released by CSCs is able to inhibit the phenotypic switching of cancer cells helping in keeping constant the number of CSCs in the bulk [3]. Plasticity of the tumor cells was shown not only in melanoma but also in other kind of tumors such as, for example, breast cancer, confirming the general capability of the cells to adapt to the environment [6]. Understanding the mechanism that drives the phenotypic switching appears, therefore, crucial to develop new therapeutic strategies.

Herein, we investigated the possible biophysical changes in human melanoma during phenotypic switching including the blebbiness index of the nuclei as a quantitative measure of nuclear shape and the interaction of polycomb group (PcG) proteins with lamins, which plays a central roles in cell identity [7]. We then considered chromatin accessibility during phenotypic switching, since the organization of accessible chromatin across the genome reflects a network of permissible physical interactions through which enhancers, promoters, insulators and chromatin-binding factors cooperatively regulate gene expression. We thus sequenced regions of open chromatin using ATAC-Seq technique, which helps to uncover chromatin packaging and other factors affecting gene expression.

Email address: caterina.laporta@unimi.it (Caterina A. M. La Porta)

Altogether our results illustrate that phenotypic switching leads to an heterogeneous population involving several crucial mechanisms including proliferation, expression of stem-like markers in connection with significant changes of nucleus morphology, interaction between PcGs and lamins and chromatin accessibility.

2. Materials and Methods

Cell culture

Human IGR39 melanoma cells were obtained from Deutsche Sammlung von Mikroorganismen und Zellkulturen GmbH. Cells were cultured in growth medium (GM): DMEM (Dulbecco's Modified Eagle's Medium (ECB7501L, EuroClone, Italy) supplemented with 10% fetal bovine serum (FBS, ECS0180D, EuroClone, Italy), 1% non-essential amminoacids (NEA, ECB3054D, EuroClone, Italy), 1% antibiotics (Penicillin/Streptomycin, Pen/Strep, ECB3001D, EuroClone, Italy), 1% L-glutamine (L-Glut, ECB3000D-20, EuroClone, Italy) at 37 °C and 5% CO_2 and 95% humidity.

Flow cytometry

Subconfluent cells were trypsinized with 0.25% trypsin/EDTA solution, centrifuged at 1200 rpm for 5 minutes at room temperature (RT), resuspended in 250 μl of ice-cold MACS buffer (1x Phosphate-buffered saline, 0.5% FBS, 2mM EDTA pH 8) and incubated with phycoerythrin (PE) anti-human CXCR6 (10μl x 10^6 cells, cod. FAB699P, R&D System, Minneapolis, MN, USA) for 1 hr, in the dark, at RT. Non-specific mouse IgG2B (10μl x 10^6 cells (C0041P, R&D System, Minneapolis, USA) was used as isotype control. For each flow cytometry evaluation, a minimum of 10^7 cells were stained and at least 5 x 10^4 events were collected and analyzed. Flow cytometry sorting and analysis was performed using a FACSAria flow cytometer (Becton, Dickinson and Company, BD, Mountain View, CA).

Cytosckeleton Pharmacological Perturbation by blebbistatin

Subconfluent cells were exposed to 25 μM Blebbistatin (B0560, Sigma-Merck, Germany) for 30 min at 37°C and 5% CO_2 and 95% humidity. Five minutes before the end of the treatment, Hoechst (1:1000, H3570, Life technology) was added to the SM (see cell culture section) to counterstain the nuclei. Immediately after the end of the treatment, fresh medium was added and cells were time-lapse imaged every 15 minutes for 1h using a Nikon A1 laser scanner confocal (63X) with a z-stack of 0.5 μm. Cell nucleus deformation was calculated using local displacements d_j as previously described [8]. Briefly, for each time point confocal z-stacks images of the nuclei were used to perform cell nucleus mesh reconstruction with the aim of the bioimage informatics platform Icy [9] on DAPI signal. In all the analyzed frames nuclei close to the borders or superimposed were manually discarded. The local displacements d_j of a triangular face j of a mesh M was calculated with respect to the corresponding mesh at previous time point. We found the matching μ that minimizes the total distance between the meshes using the Hungarian algorithm [10] as implemented by SciPy library [11] function *scipy.optimize.linear_sum_assignment*. For each face, we computed the displacement vectors of each vertex and local displacement d_j as the average projection over the normal vectors. For each cell, the standard deviation $\sigma(d)$ of local displacements d_j over all the faces can be used as a proxy of deformation. Heterogeneous or localized morphological changes are associated to large values of $\sigma(d)$ while low values of $\sigma(d)$, are obtained when the changes are homogeneous over the nucleus surface.

Immunofluorescence

Subconfluent cells grown on glass coverslips were fixed with 3.7% paraformaldehyde in phosphate-buffered saline (PBS) for 10 min, permeabilized with 0.5% Triton X-100 in PBS for 5 min at room temperature (RT), and incubated with 5% BSA in PBS for 1 h. The cells were stained with anti-H3K4met3 (1:100, Abcam, ab8580) or anti-CXCR6 (1:400, Abcam, ab8023) or anti-Ki67(1:1000,Abcam,ab16667) or anti-panlamin (1:50, Abcam, ab20740) overnight at 4°C and incubated with the secondary antibody

(1:250, Abcam, ab150077) for 1 h at RT. The nuclei were counterstained with DAPI, and the slides were mounted with Pro-long antifade reagent (cod. P36931, Life Technologies). The images were acquired with Nikon A1 laser scanner confocal (63X).

Analysis of Immunofluorescence of Ki67 and CXCR6 assay

For each image, segmentation was perfomed using ICY bioimage analysis HK-means plugin (v.1.9.5) [9] and cells at the border were manually discarded. For each nucleus, we calculated average Ki67 signal over the pixel superimposed to DAPI signal and CXCR6 average intensity outside the nucleus.

Proximity ligation assay and quantification

Subconfluent cells were fixed on slides with ice-cold 100% methanol for 5 min at at -20°C and incubated with Duolink Blocking Solution for 60 minutes at 37°C in a humidity chamber. Slides were then incubated in a humidity chamber overnight at 4°C with panlamin (1:50, mouse ab20740, Abcam, Cambridge, UK) and SUZ12 (1:800, rabbit mAb 3737, Cell Signaling Technology, Danvers, MA) or BMI1 (1:600, rabbit mAb 6964, Cell signaling Technology, Danvers, MA). After washing, the samples were incubated in a preheated humidity chamber for 1 h at 37°C with anti-rabbit PLUS and anti-mouse MINUS PLA probes diluted 1:5. PLA probes generate a fluorescent signal when bound to two different primary antibodies, raised in different species, that recognize two antigens in close proximity (less than 40 nm). All the antibodies were diluted in Duolink Antibody Diluent. Ligation and amplification steps were performed according to manufacturer's instructions. Slides were mounted with Duolink In Situ Mounting Medium with DAPI (DUO82040; Sigma-Merck, Germany). The images were acquired with Nikon A1 laser scanner confocal (63X). Immunofluorescence images were analyzed using existing and customized plugins of the bioimage platform Icy (v.1.9.4 and 1.9.5[9]) and custom python scripts as previously described in [8]. Briefly, duolink spot recognition was performed separately on each nucleus with a semi-automatic protocol involving HK-means thresholding (ICY Thresholder plugin). The minimum size of each accepted spot was set to 70 px. In all the analyzed frames nuclei close to the borders or superimposed were manually discarded.

2D analysis of nuclear morphology: blebbiness index

Nuclear morphology was evaluated using blebbiness index on cells fixed and stained with DAPI and acquired by Nikon A1 laser scanner confocal (63X) as previously described [8]. Briefly, nuclear segmentation was performed in MATLAB lMATLAB and the curvature of nuclei along each point of their perimeter was estimated using UnivariateSpline function from SciPy python library. Negative value of the curvature in two-dimensional images is a signal of abnormal nuclear morphology. We define the blebbiness index ϕ as the weighted fraction of negative curvature along the perimeter of each nucleus. Larger values of ϕ correspond to nuclei with irregular shape, while small values indicate smooth contours.

2D analysis of chromatin conformation

Chromatin conformation was evaluated using projection of three dimensional images of cells fixed on glass coverslips and stained with DAPI and acquired with Nikon A1 laser scanner confocal (63X). DAPI homogeneity was evaluated using Haralick texture features using grey-level co-occurrence matrix [12]. Homogeneity corresponds to the inverse difference moment of an image and only the values close to the diagonal are relevant. Images were converted to 8-bits. For each image, segmentation was perfomed using ICY bioimage analysis HK-means plugin and and homogeneity inside the nucleus was calculated. Cells at the border were manually discarded and pixels with intensity less than 5 were considered as background.

Assay for Transposase-Accessible Chromatin using sequencing (ATAC-seq)

Cells were harvested and suspended in a homogenous single cell suspension in standard growth medium (SM). For each condition, $5 \cdot 10^4$ cells were centrifugated at 500 X g for 5 min at 4°C. Cell pellet was then resuspended in 50μl of cold lysis buffer (10 mM Tris-HCl, pH 7.4, 10 mM NaCl, 3 mM $MgCl_2$, 0.1% Nonidet P40 (Sigma)) and immediately spinned down at 500 X g for 5 min at 4°C. This step provides lysis of cells with non-ionic detergent and generates of a crude nuclei preparation. After discarding the supernatant, the cell pellet was set on ice and resuspended in the transposition reaction mix containing 25 μl TD -2x reaction buffer (cod.15027866, Illumina) and 2.5 μl Tagment DNA Enzyme 1: (cod.15027865, Illumina) and 22.5 μl of Nuclease Free water.The resuspended pellet was then incubated for 30 min at 37°C. Finally, DNA was purified and eluted in in 10μl elution buffer (10 mM Tris buffer, pH 8) using a Qiagen MinElute PCR Purification Kit (Qiagen, catalog 28004)according to manufacturer's istructions. Purified DNA was stored at -20°C until library preparation.

Fragment size between 100/2500 bps were sequenced using an Illumina NextSeq 500DX System (Illumina, San Diego, CA) in a 2 X 75 pair end format, 60MX reads/sample. The raw sequence files generated underwent quality control analysis using FastQC (http://www.bioinformatics.babraham.ac.uk/publications.html). Sequencing Nextera Indexes were trimmed using Trimgalore (v. 0.4.4) and hard-trimmed to reduce reads size to 60bps. Bowtie2 [13] in sensitive mode was used to align sequences on Human Genome (GRCh38, GCA_000001405.15, https://www.ncbi.nlm.nih.gov/).

Genrich [14] and ATAC-QC [15] were used to peak calling (corrected p-values < 0.05), bed files generation and PCA analysis. Bedtools intersect (with option -a) [16] was used for deletion of Encode blacklist regions [17] and mapping on intersection with lamina-associated domains (LADs). List of constitutive LADs (cLADs), constitutive inter-LADs (ciLADs), facultative LADs (fLADs), and facultative inter-LADs (fiLADs) regions in nine human cell lines was obtained from LAD atlas(v.2) [18, 19]. Differential expression analysis on the peaks was performed using EdgeR[20]. P-values < 0.01 is used to identify differentially expressed peaks.

Western Blot

Subconfluent cells were lysed by boiling in a modified Laemmli sample buffer (2% SDS, 20% glycerol, and 125 mM Tris-HCl, pH 6.8). The protein concentration was measured by DC Protein Assay Kit (BioRad). Equal amount of proteins were loaded on 10% SDS-PAGE gel and transferred to a PVDF membrane (Trans-Blot Turbo Mini PVDF, BioRad). After blocking with 5% BSA/0.5% Tween20 in PBS for 1h at RT, the sheets were incubated with primary antibodies anti-SUZ12 (1:2000, rabbit, cod. 3737, Cell Signalling Technonologies) or BMI1 (1:2000,rabbit, cod. 6964,Cell Signalling Technonologies) or Lamin A/C (1:2000, mouse, cod. 2032, Cell Signalling Technonologies) or BMI1 (1:2000,rabbit, cod. 6964,Cell Signalling Technonologies) overnight at 4°C. Sheets were incubated with secondary antibodies for 1hr at RT. β-tubulin (1:5000,mouse, cod. cod T8328, Sigma) was used as housekeeping reference.

Statistical analysis

Unpaired two tails t-test and unpaired two-sided wilcoxon test were used to assess statistical significance as reported in the captions.

Results

Biophysical nuclear changes during phenotypic switching and proliferative and stem-like markers expression

We investigated the possible biophysical changes during phenotypic switching of the nucleus such as blebbiness and DNA homogeneity in connection with proliferation and stem-related markers using Ki-67 [21] and CXCR6, respectively [4].

First, we sorted out the negative population of IgR39 melanoma cells for CXCR6, a melanoma stem cell marker [4]. In fact, in a recent paper, we showed that the CXCR6 negative cells can switch to

positive ones by re-expressing CSC markers including CXCR6 with an overshoot 10 days after sorting [4]. Therefore, herein, we quantifies before the overshoot (72h after sorting) and at the overshoot, the morphology o the nucleus using the blebbiness index [8] and the distribution of DAPI signal inside the nuclei quantifying the homogeneity of the image. (see Materials and Methods for more details). As shown in figure 1, we found an increase of blebbiness and DAPI homogeneity at the overshoot. It has been reported in the literature that the formation of nuclear blebs, together with other morphological features, could be an indicator of genetic instability and intratumor heterogeneity, independently by the cytogenetic complexity and the grade of malignancy of the tumor [22]. Moreover, DAPI signal intensity distribution is indicative of the chromatin status, the latter changes during cell cycle progression and is related to the nuclear stiffness [23, 24, 25]. A large homogeneity value indicates that pixels close in space have similar intensity values. This is the case when chromatin is condensed in specific regions and in presence of nucleoli so that DAPI signal is particularly homogeneous inside those regions. At the opposite, when there are no large bright spots of DAPI, the intensity of two pixels close one to the other is not related, they have different values, and DAPI homogeneity results lower. The presence of large regions with constant DAPI signal has been thus related to large domains of eu/heterocromatin and allows us to evaluate the presence of this patterning with minimal modification of the images when compared to other methods [23].

Under the same conditions, we checked the cell proliferation status using Ki67 [21] during the phenotypic switching as well as the level of expression of the stem-like marker CXCR6 showing, according to [4], an increase of both parameters at the overshoot (Figure 2).

Lamins, cytoskeleton and chromatin organization during pheotypic switching

It is known that lamins, which are of three different types (lamin A, B and C), play an important role with respect to the elastic and viscoelastic response of the nucleus [26, 27, 28], affecting both gene expression and cell fate [29]. Nuclear shape is not exclusively dependent on nucleus intrinsic structural and mechanical properties but it is rather determined by the interplay existing between the nuclear lamina acting as nuclear skeleton, the chromatin and the cytoskeleton. Herein, we studied the contribution of cytoskeletal activity on the nuclear shape during phenotypic switching by measuring time-dependent shape fluctuations after perturbation with blebbistatin, a well-know myosin inhibitor [8]. To this end, after a 30min exposure to blebbistain we followed the cells by time lapse for 1 hour measuring the local displacement of the nuclei which indicates how much each node of the mesh is displaced from the previous time-point [8]. To quantify the fluctuations of the mesh at each instance, we then computed the standard deviation of d_j as a function of time. As shown in Fig.3, while no changes in the amplitude of nuclear fluctuations are present in the untreated cells (Fig.3a), CXCR6-negative cells 10 days after sorting, displayed a significant reduction of the nuclear envelope fluctuation after exposure with blebbistatin with respect to untreated (Fig.3d)) or WT cells (Fig.3f,4b). These results seem to suggest that the cells during phenotypic switching have a change in the stiffness due to a different organization of chromatin/lamin/cytoskeleton interaction.

To better understand the interaction between lamins and chromatin, we focused on polycomb group (PcG) proteins. These are transcriptional repressors which play a central roles in many biological functions including cell identity maintenance through the interaction with lamins [7]. There are two complexes PRC1 and PRC2 that can act in synergy or independently from each other affecting different genes [7]. PRC2 is recruited for targeting genomic region to be silenced by performing histone H3 lysine 27 for mono-, di- and trimethylation (H3K27me1, 2, 3), while PRC1 is required for stabilizing this silencing by the mono-ubiquitination of lysine 119 of histone H2A (H2AK119ub1) and also perform ubiquitination-independent chromatin compaction [8, 30]. Using proximity ligation assay (PLA), we quantified the interaction between SUZ12 (belonging to PCR2) or BMI1 (belonging to PCR1) with pan-lamins before (72h after sorting) or at the overshoot (10 days after sorting) [4]. As shown in Fig.5, we found a significant reduction in BMI1-lamins interactions (Fig5a) and an increased interaction for SUZ12/lamins (Fig.5b) at the overshoot. These changes are unrelated to the level of expression either of BMI1, SUZ12 as shown

by western blot (Fig.6). In contrast, we found that the level of expression of lamin A and B decreases significantly at the overshoot (Fig.7).

We also found a significative different expression in higher-order chromatin organization using H3K4met3 as euchromatin marker (Figure 5c).

Chromatin accessibility during overshoot by ATAC-seq

To investigate possible changes in chromatin accessibility across the genome during the phenotypic switching, we carried out ATAC-seq analysis (see Materials and Methods section for more details).

As shown in Fig.8a, 72h after sorting and at the overshoot the cells show a decrease of signal related to di- and tri-nucleosomal regions with an increase of small-size fragments. 72h after sorting cells show an intermediate status between the other two considering peak positioning and abundance (Fig.8b-c) . It is known that in metazoan cell nuclei, hundreds of large chromatin domains are in close contact with the nuclear lamina. Such lamina-associated domains (LADs) are thought to provide chromosomes with a basic backbone structure, helping the organization of chromosomes inside the nucleus and being associated with gene repression [31]. Furthermore, there are two classes of LADs described in the literature: those that interact with the lamins in all cell types, designated as constitutive LADs that seems to contribute to a basal chromosome architecture, and LADs that are cell-type specific that are called facultative [32].

We thus analyzed the peaks distribution in costitutive and facultative LADs (cLAD and fLAD, respectively) and inter-LADs (ciLAD and fiLAD, respectively). As show in Fig.8d, a small fraction of ATAC-seq peaks are located in LADs regions, either constitutive or facultative. However, there is a general decrease of signal associated to these regions 72h after sorting (Fig.8e). In contrast, at the overshoot there is an increase of fLAD and both ci- and fi-LADS, suggesting increased accessibility of the chromatin in these regions.

Discussion

Tumor plasticity is nowadays the key problem for cancer metastasis and for the identification of new therapeutic strategies. Cancer cell plasticity promotes cancer cell diversity and contributes to intra-tumor heterogeneity, allowing cancer cells under specific environmental conditions to shift dynamically between a differentiated state, with limited tumorigenic potential, and an undifferentiated or CSC-like state, which is responsible for long-term tumor growth [33] . Cancer cell plasticity has been linked to the EMT program and relies not only on cell-autonomous mechanisms, but also on signals provided by the tumor microenvironment and/or induced in response to therapy [4, 34]. In the last few years, our group investigated in depth the complex mechanisms underlying phenotypic switching in human melanoma focusing in particular on the role of miRNA [4]. Melanoma is a very aggressive tumor poor responsive to therapy when metastatic [35]. We found that sorting human melanoma negative cells for CSC's markers, including CXCR6, and following them during the time, the cells were able to switch back to CSCs rebuilding an heterogenous population [4].

Herein, we further investigated the mechanisms behind the formation of an heterogenous population starting from negative CXCR6 cells investigating possible biophysical changes occurring at the level of nucleus. To this end, we measured the blebbiness index of the nucleus during phenotypic switching as well as the DNA homogeneity. We here show that both these factors which are related to genetic instability and intratumor heterogeneity[22], increase at the overshoot in connection with a higher proliferative capacity measured quantifying the level of expression of Ki67 and an increase in the level of expression CXCR6 a CSC's markers [4].

Since it is known that lamins play a critical role in response to elastic and viscoelstic response [26, 27, 28], we further investigated the possible differences in the organization of chromatin/lamins/cytoskeleton. Firstly, we investigated the nuclear deformations during phenotypic switching measuring the shape fluctuations after short perturbation with an inhibitor of myosin, blebbistatin [8]. We found that the nucleus of cells at overshoot are stiffer after blebbistain treatment when compared with untreated cells, suggesting

that they have a different organization in chromatin/lamins/cytoskeleton. Second, we investigated the impact of phenotypic switching on the organization of the complex polycomb-lamin with the PLA assay [8]. We found that while the SUZ12-lamins interaction increases (Suz12 belonging to PRC2), BMI1-lamins decreases (BMI1 belonging to PRC1). In addition, we did not find any changes in the level of expression of polycombs and lamin C, while a slight decrease of lamin A and lamin B occurs at the overshoot. In breast cancer, overexpression of EZH2 was shown to increase mammosphere formation and self-renewal ability in CSCs [36, 37]. Furthermore in glioblastoma, the loss of H3K27me3 was shown to lead to aberrant activation of Wnt pathway which is required for tumorigenicity and CSC maintenance [38]. More recently, PRC2 was shown to be a key regulators of brain tumor plasticity [39]. It is well known that SUZ12/EZH2 mediates transcriptional repression of target genes via the trimethylation of lysine 27 of histone 3 (H3K27me3) [40], which appears also to be upregulated in many cancers and its enhanced expression is associated with invasion, migration and stemness [41].

Proper functioning of chromatin involves a network of interactions among molecular complexes that modify chromatin structure and organization to affect the accessibility of DNA to transcription factors leading to the activation or repression of the transcription of target DNA loci. Based on its structure and compaction state, chromatin is categorized into euchromatin, characterized by active genes, and heterochromatin, transcriptionally less active and associated with gene silencing, being less accessible than euchromatin. We thus investigated in more depth the higher-order chromatin organization using H3K4met3 as euchromatin probe, showing a decrease of this marker in melanoma cells at the overshoot. This confirms that at the overshoot, where there is the peak of proliferation and re-expression of CSC's markers, heterogeneity is already established and cancer cells are starting to decrease the chromatin accessibility DAPI homogeneity, increase of blebbiness and formation of heterochromatin [5] [5].

Altogether, our results shed light on the mechanisms of tumor heterogeneity showing that an important remodeling of the chromatin/lamin/cytoskeleton occurs during the phenotypic switching of melanoma cells, affecting the transcriptional activity of the cells and thereby their phenotype.

Acknowledgments

We thank S. Zapperi for critical reading of the manuscript and F. Font-Clos for useful discussions.

Funding

This work was supported by a grant from the Fondazione AIRC per la Ricerca sul Cancro (grant IG 21558).

Figures

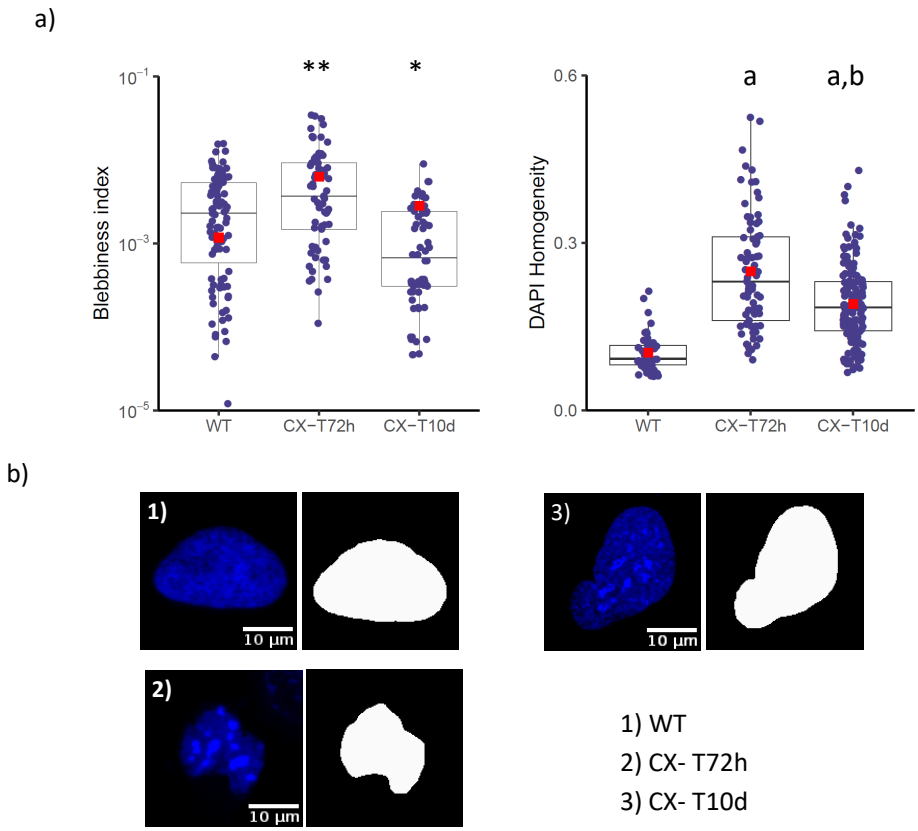

Figure 1: a) Quantification of blebbiness index and DAPI homogeneity in WT cells and in CXCR6 sorted negative cells analysed 72h or 10 days after. Blebbiness index was obtained computing the curvature fluctuations as described in the Materials and Methods section. DAPI homogeneity was used to evaluate chromatin status,as described in Materials and Methods. For each condition, 8 to 12 different images were acquired. The number of nuclei considered is the followed: WT 49, T72h 77, T10d 136. Bars in boxplots indicate minimum and maximum quartiles, boxes are first and third quartiles. Red squares indicate average value. Statistical significance was evaluated using Kolmogorov-Smirnov test (** $p=6\cdot10^{-3}$ for CX-T72h with respect WT, * $p=2\cdot10^{-2}$ for CX-T10d with respect WT, a:$p< 10^{-15}$ for CX-T72h and CX-T10d with respect WT, b : $p< 10^{-3}$ for CX-T72h with respect CX-T10d). b) Representative images of WT, CXCR6 negative nuclei 72h and 10 days after sorting stained with DAPI (left, blue) with the corresponding contour to highlight nuclear curvature (right, white).

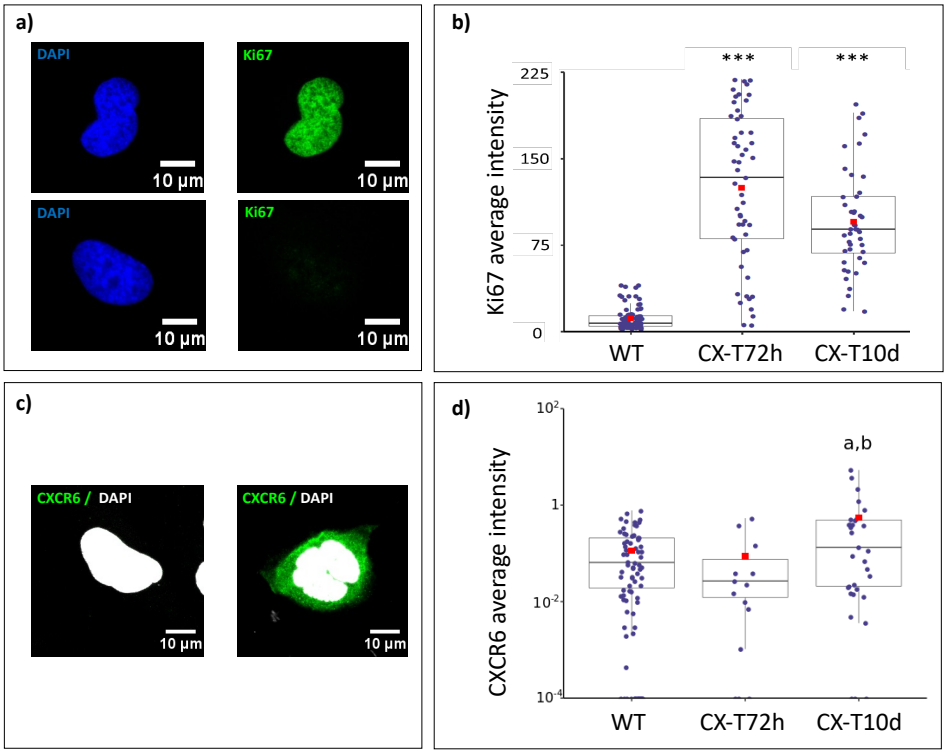

Figure 2: Panel a: representative images of Ki67 staining. Cells were fixed with 3.7% paraformaldehyde and incubated with polyclonal anti-Ki67 antibody (1:1000, Abcam, Ab16667) 4°C, overnight. Then the cells were incubated with the secondary antibody (1:250, ab150077, AbCam) for 1 h at room temperature and the nuclei counterstained with DAPI. The slides were mounted with Pro-long anti fade reagent (P7481, Life Technologies) and the images acquired with a Nikon A1 laser scanner confocal microscope. Cytoplasmic Ki67 signal is set to zero and neglected in the analysis. Panel b : the graphs represents the average intensity of Ki67 signal, calculated inside the nucleus as described in the Materials and Methods in WT, CXCR6-negative cells 72h or 10 days after sorting. The statistical significance was calculated using the Wilcoxon-test (*** p¡10^{-14} for CX-T72h, CX-T10d with respect WT). Panel c : representative images of CXCR6 negative cell and CXCR6 expressing cell. Cells were fixed with 3.7% paraformaldehyde and incubated with polyclonal anti-CXCR6 antibody (1:400, Abcam, Ab8023) 4°C, overnight. Then the cells were incubated with the secondary antibody (1:250, ab150077, AbCam) for 1 h at room temperature and the nuclei counterstained with DAPI. The slides were mounted with Pro-long anti fade reagent (P7481, Life Technologies) and the images acquired with a Nikon A1 laser scanner confocal microscope. CXCR6 signal inside the nucleus is neglected. Panel d : the graphs represents the average intensity of CXCR6 signal, calculated excluding nuclear region in WT cells, CXCR6-negative cells 72h and 10days after sorting. Bars in boxplots indicate minimum and maximum quartiles, boxes are first and third quartiles. Red squares indicate average value. The statistical significance was calculated using the Wilcoxon-test (a : p=0.015 for CX-T10d with respect to WT; b: p=0.043 for CX-T10d with respect to CX-T72h)

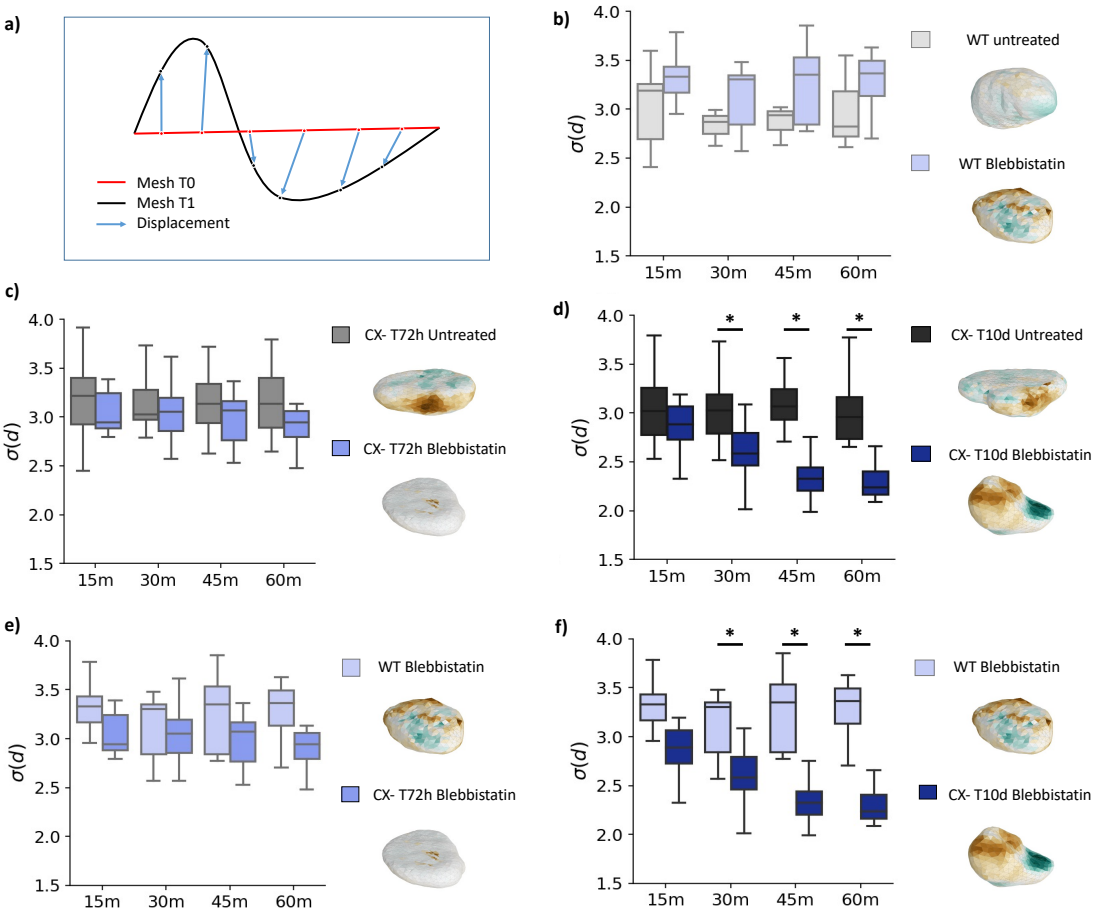

Figure 3: Panel a: Schematic representation of the method used to quantify the nuclear local displacements. Given the meshes of the same nucleus at two different timepoints (i.e. T0 and T1), the vectors v_i is identified by the algorithm and used to compute $\sigma(d)$; see Materials and Methods for details. Panel b-f : Boxplot of $\sigma(d)$ overtime for WT and CXCR6 negative cells 72h and 10 days after sorting, untreated or exposed to 25μM blebbistatin for one hour and then wash out (see Materials and Methods for more details). Statistical significance was calculated using t-Test (* $p < 10^{-5}$). Data have been collected over at least three independent experiments. Error bars in boxplots indicate minimum and maximum quartiles, boxes are first and third quartiles.

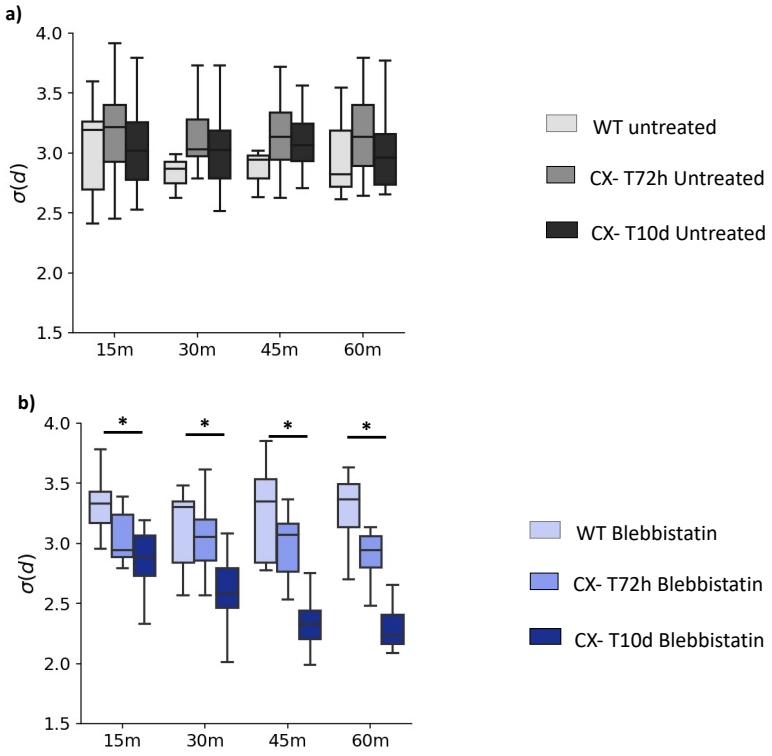

Figure 4: Boxplot of $\sigma(d)$, used as proxy of nuclear shape deformation, as function of time for IgR39 WT and CXCR6 negative cells at 3 and 10 days after sorting maintained in standard growth medium (panel a) or exposed to blebbistatin (panel b). Statistical significance was calculated using t-Test (* $p < 10^{-5}$).

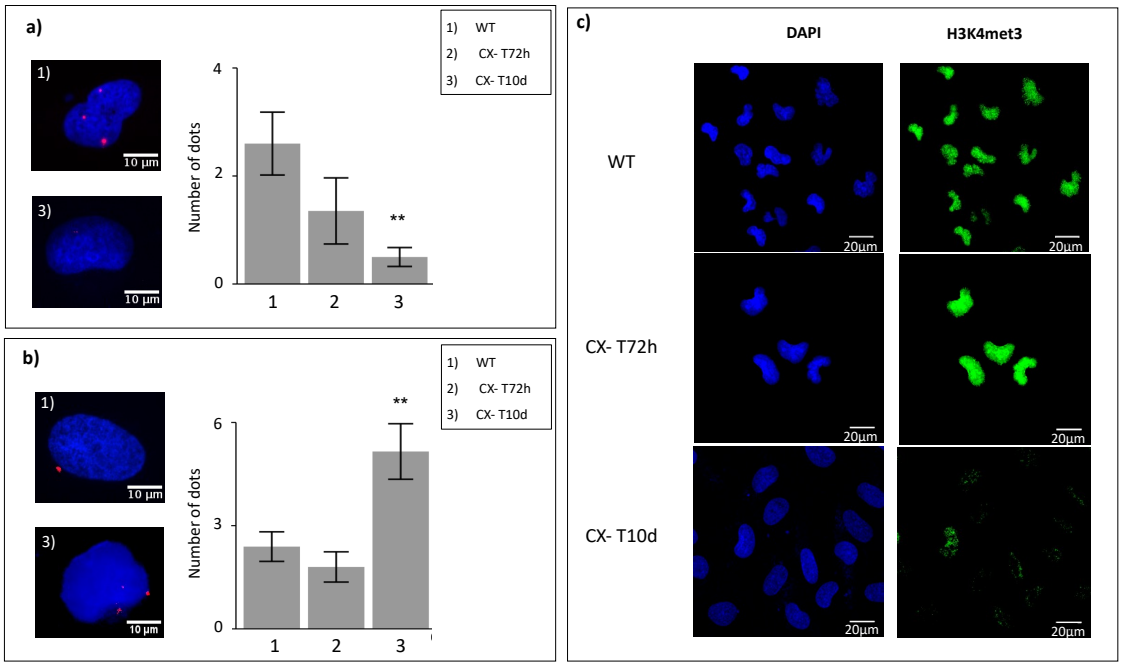

Figure 5: PRCs interactions with nuclear lamina are affected during phenotypic switching. The tethering between nuclear lamina and PCRs components was quantified by the proximity ligation assay measuring the interaction between lamins using a panlamin antibody (1:50, mouse ab20740, Abcam) and BMI1 (1:600, rabbit mAb 6964, Cell signaling Technology) or SUZ12 (1:800, rabbit mAb 3737, Cell Signaling Technology), in panel a and b, respectively. The number of fluorescent red spots, each representing lamins interactions with BMI1 or SUZ12, were quantified as described in the Materials and Methods section. The analysis was carried out on at least 17 nuclei for each condition, collected over at least three replica. Statistical significance is established by the unpaired t-test method (**=p-value <0.01). Error bars indicates SE. Panel c) : Immunofluorescence of H3K24met3 in WT and CXCR6 negative cells 72h and 10 days after sorting. Cells were fixed with 3.7% paraformaldehyde, permeabilized with 0.1% Triton-X100 in PBS for 15 min at RT and incubated overnight at 4°C with t anti-H3K4met3 antibody (1:100, Abcam, ab8580).The samples were then incubated with FITC anti-Rabbit (1:250, ab150077, AbCam) for 1 h at RT and mounted with Pro-long anti-fade reagent (P7481, Life Technologies) with DAPI to stain the nuclei.

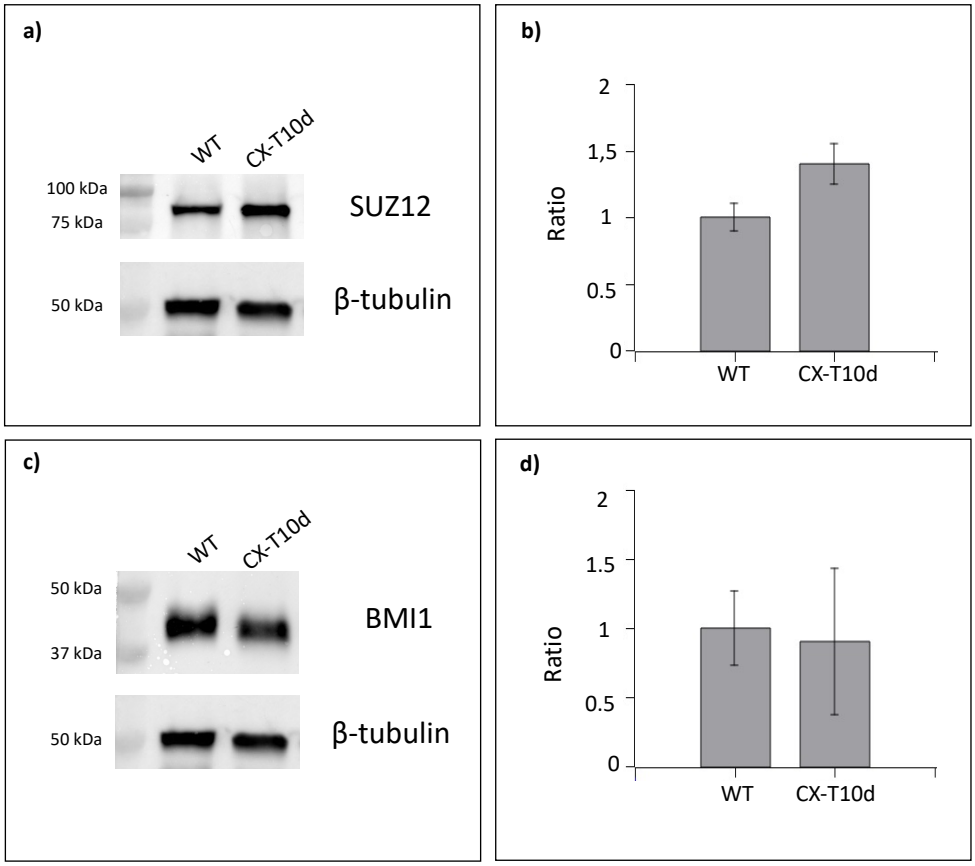

Figure 6: Panel a and c: Representative Western blots for SUZ12 and BMI1 expression in WT cells and CXCR6-negative cells 10 days after sorting. Equal amount (20 μg) of protein were loaded on 10% polyacrylamide gel, transferred on PVDF and incubated with BMI1 (1:2000,rabbit, cod. 6964,Cell Signalling Technonologies) or SUZ12 (1:2000, rabbit, cod. 3737, Cell Signalling Technonologies) . β-tubulin was used as housekeeping. Panel b and d: Mean of densitometric analysis of two independent western blot of SUZ12 and BMI1. The Y axis represents the ratio between the densitometric value of SUZ12 or BMI1 with respect to the housekeeping.

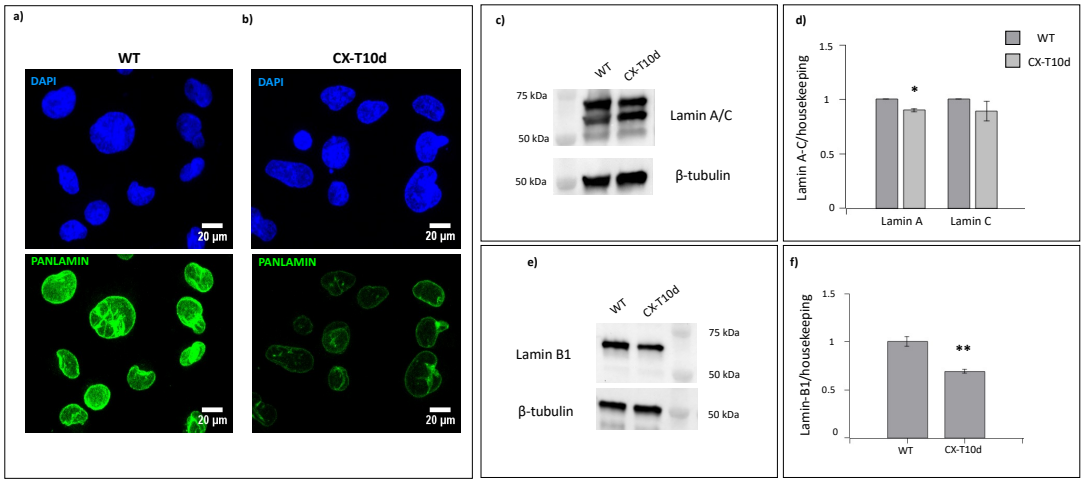

Figure 7: Panel a and b : Representative images of nuclear lamina stained with anti-Panlamin antibody in IgR39 unsorted cells (WT) and CXCR6-negative cells 10 after sorting, respectively. Cells were fixed with 100% methanol and incubated with anti-PanLamin antibody (1:50,mouse Abcam, Ab20740) 4°C, overnight. Then the cells were incubated with the secondary antibody (1:250, ab150113, AbCam) for 1 h at room temperature and the nuclei counterstained with DAPI. The slides were mounted with Pro-long anti fade reagent (P7481, Life Technologies) and the images acquired with a Nikon A1 laser scanner confocal microscope. Panel c and e : Representative Western blots showing Lamin A/C or Lamin B1 expression in IgR39 cells and CXCR6-negative cells 10 days after sorting. Equal amount of protein (20 μg) were loaded on 10% polyacrylamide gel, transferred on PVDF and incubated with Lamin A/C (1:2000, mouse, cod. 2032, Cell Signalling Technonologies) or Lamin B1 (1:200, rabbit, ab16048) . β-tubulin was used as housekeeping. Panel d and f: Mean of densitometric analysis of two independent western blot of Lamin A/C and Lamin B1 performed with ImageJ. The Y axis represents the ratio between the densitometric value of Lamin A/C or Lamin B1 with respect housekeeping. The statistical significance was calculated using the T.test (* p¡0,05 for CX-T10d with respect WT, ** p¡10^{-4} for CX-T10d with respect WT)

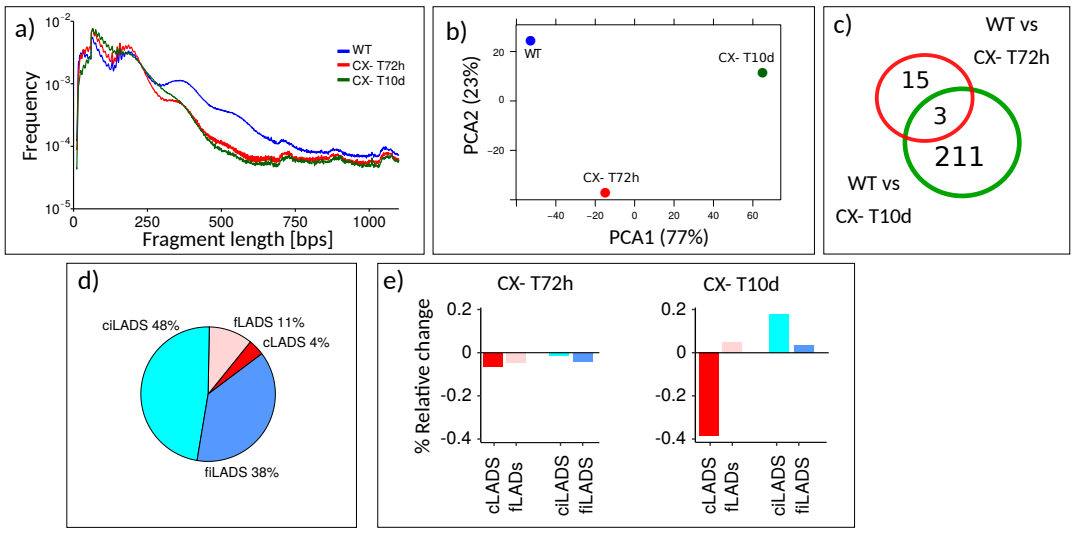

Figure 8: a)Insert size distributions of ATAC-seq data for WT and CXCR6 negative cells 72h and 10 days after sorting. Fragments below 100bps represent the open chromatin, peaks at $\approx$ 200/400/600 bps represent mono-, di- and tri-nucleosomal regions. b) Principal component analysis of ATAC-seq peaks counts for the three experimental conditions. ATAC-seq profile of CXCR6 negative cells 72h after sorting is closer to WT profile compared to negative cells after 10 days , as confirmed by analysis of differentially expressed peaks (c). d-e) Distribution of peaks in constitutive or facultative LADs (cLADs,fLADS) and inter-LADs regions (ciLADs, fiLADS) and percentage of peaks gained or lost in each region in CXCR6 negative cells compared to WT. CXCR6 Negative cells 10d acquire peaks in non-LAD regions while signal in cLADs regions decreases compared to WT cells.

[1] E. Monzani, F. Facchetti, E. Galmozzi, E. Corsini, A. Benetti, C. Cavazzin, A. Gritti, A. Piccinini, D. Porro, M. Santinami, G. Invernici, E. Parati, G. Alessandri, C. A. M. La Porta, Melanoma contains cd133 and abcg2 positive cells with enhanced tumourigenic potential, Eur J Cancer 43 (5) (2007) 935–46. doi:10.1016/j.ejca.2007.01.017.

[2] C. A. M. La Porta, S. Zapperi, J. P. Sethna, Senescent cells in growing tumors: population dynamics and cancer stem cells, PLoS Comput Biol 8 (1) (2012) e1002316. doi:10.1371/journal.pcbi.1002316.

[3] M. C. Lionetti, F. Cola, O. Chepizhko, M. R. Fumagalli, F. Font-Clos, R. Ravasio, S. Minucci, P. Canzano, M. Camera, G. Tiana, S. Zapperi, C. A. M. L. Porta, Microrna-222 regulates melanoma plasticity, J Clin Med 9 (8). doi:10.3390/jcm9082573.

[4] A. L. Sellerio, E. Ciusani, N. B. Ben-Moshe, S. Coco, A. Piccinini, C. R. Myers, J. P. Sethna, C. Giampietro, S. Zapperi, C. A. M. La Porta, Overshoot during phenotypic switching of cancer cell populations, Sci Rep 5 (2015) 15464. doi:10.1038/srep15464.

[5] J. Wouters, Z. Kalender-Atak, L. Minnoye, K. I. Spanier, M. De Waegeneer, C. Bravo González-Blas, D. Mauduit, K. Davie, G. Hulselmans, A. Najem, M. Dewaele, D. Pedri, F. Rambow, S. Makhzami, V. Christiaens, F. Ceyssens, G. Ghanem, J.-C. Marine, S. Poovathingal, S. Aerts, Robust gene expression programs underlie recurrent cell states and phenotype switching in melanoma, Nat Cell Biol 22 (8) (2020) 986–998. doi:10.1038/s41556-020-0547-3.

[6] G. M. Wahl, B. T. Spike, Cell state plasticity, stem cells, emt, and the generation of intra-tumoral heterogeneity, NPJ Breast Cancer 3 (2017) 14. doi:10.1038/s41523-017-0012-z.

[7] C. Lanzuolo, V. Orlando, Memories from the polycomb group proteins, Annu Rev Genet 46 (2012) 561–89. doi:10.1146/annurev-genet-110711-155603.

[8] M. C. Lionetti, S. Bonfanti, M. R. Fumagalli, Z. Budrikis, F. Font-Clos, G. Costantini, O. Chepizhko, S. Zapperi, C. A. La Porta, Chromatin and cytoskeletal tethering determine nuclear morphology in progerin-expressing cells, Biophysical Journal 118 (9) (2020) 2319–2332. doi:https://doi.org/10.1016/j.bpj.2020.04.001.
URL https://www.sciencedirect.com/science/article/pii/S0006349520303015

[9] F. de Chaumont, S. Dallongeville, N. Chenouard, N. Hervé, S. Pop, T. Provoost, V. Meas-Yedid, P. Pankajakshan, T. Lecomte, Y. Le Montagner, T. Lagache, A. Dufour, J.-C. Olivo-Marin, Icy: an open bioimage informatics platform for extended reproducible research, Nat Methods 9 (7) (2012) 690–6. doi:10.1038/nmeth.2075.

[10] H. W. Kuhn, The hungarian method for the assignment problem, Nav. Res. Logist. 52 (1) (2005) 7–21.

[11] E. Jones, T. Oliphant, P. Peterson, SciPy: Open source scientific tools for Python (2001).

[12] R. M. Haralick, Statistical and structural approaches to texture, Proceedings of the IEEE 67 (5) (1979) 786–804. doi:10.1109/PROC.1979.11328.

[13] B. Langmead, S. Salzberg, Langmead b, salzberg sl.. fast gapped-read alignment with bowtie 2. nat methods 9: 357-359, Nature methods 9 (2012) 357–9. doi:10.1038/nmeth.1923.

[14] [online] (2021). [link].

[15] J. Ou, H. Liu, J. Yu, M. Kelliher, L. Castilla, N. Lawson, L. Zhu, Atacseqqc: A bioconductor package for post-alignment quality assessment of atac-seq data, BMC Genomics 19. doi:10.1186/s12864-018-4559-3.

[16] A. R. Quinlan, I. M. Hall, BEDTools: a flexible suite of utilities for comparing genomic features, Bioinformatics 26 (6) (2010) 841–842. arXiv:https://academic.oup.com/bioinformatics/article-pdf/26/6/841/16897802/btq033.pdf, doi:10.1093/bioinformatics/btq033.
URL https://doi.org/10.1093/bioinformatics/btq033

[17] H. Amemiya, A. Kundaje, A. Boyle, The encode blacklist: Identification of problematic regions of the genome, Scientific Reports 9 (2019) 9354. doi:10.1038/s41598-019-45839-z.

[18] J. Kind, L. Pagie, S. Vries, L. Nahidiazar, S. Dey, M. Bienko, Y. Zhan, B. Lajoie, C. de Graaf, M. Amendola, G. Fudenberg, M. Imakaev, L. Mirny, K. Jalink, J. Dekker, A. Oudenaarden, B. Steensel, Genome-wide maps of nuclear lamina interactions in single human cells, Cell 163. doi:10.1016/j.cell.2015.08.040.

[19] J. Kind, L. Pagie, S. Vries, L. Nahidiazar, S. Dey, M. Bienko, Y. Zhan, B. Lajoie, C. de Graaf, M. Amendola, G. Fudenberg, M. Imakaev, L. Mirny, K. Jalink, J. Dekker, A. Oudenaarden, B. Steensel, Genome-wide maps of nuclear lamina interactions in single human cells, Cell 163. doi:10.1016/j.cell.2015.08.040.

[20] M. D. Robinson, D. J. McCarthy, G. K. Smyth, edger: a bioconductor package for differential expression analysis of digital gene expression data, Bioinformatics 26 (1) (2010) 139–40. doi:10.1093/bioinformatics/btp616.

[21] R. Sales Gil, P. Vagnarelli, Ki-67: More hidden behind a 'classic proliferation marker', Trends Biochem Sci 43 (10) (2018) 747–748. doi:10.1016/j.tibs.2018.08.004.

[22] D. Gisselsson, J. Björk, M. Höglund, F. Mertens, P. Dal Cin, M. Akerman, N. Mandahl, Abnormal nuclear shape in solid tumors reflects mitotic instability, Am J Pathol 158 (1) (2001) 199–206. doi:10.1016/S0002-9440(10)63958-2.

[23] S.-J. Heo, S. D. Thorpe, T. P. Driscoll, R. L. Duncan, D. A. Lee, R. L. Mauck, Biophysical regulation of chromatin architecture instills a mechanical memory in mesenchymal stem cells, Sci Rep 5 (2015) 16895. doi:10.1038/srep16895.

[24] S. M. Bondarenko, I. V. Sharakhov, Reorganization of the nuclear architecture in the drosophila melanogaster lamin b mutant lacking the caax box, Nucleus 11 (1) (2020) 283–298. doi:10.1080/19491034.2020.1819704.

[25] M. W. Linhoff, S. K. Garg, G. Mandel, A high-resolution imaging approach to investigate chromatin architecture in complex tissues, Cell 163 (1) (2015) 246–55. doi:10.1016/j.cell.2015.09.002.

[26] J. Lammerding, R. D. Kamm, R. T. Lee, Mechanotransduction in cardiac myocytes, Ann N Y Acad Sci 1015 (2004) 53–70. doi:10.1196/annals.1302.005.

[27] J. Lammerding, Mechanics of the nucleus, Compr Physiol 1 (2) (2011) 783–807. doi:10.1002/cphy.c100038.

[28] J. Lammerding, L. G. Fong, J. Y. Ji, K. Reue, C. L. Stewart, S. G. Young, R. T. Lee, Lamins a and c but not lamin b1 regulate nuclear mechanics, J Biol Chem 281 (35) (2006) 25768–80. doi:10.1074/jbc.M513511200.

[29] J. Swift, I. L. Ivanovska, A. Buxboim, T. Harada, P. C. D. P. Dingal, J. Pinter, J. D. Pajerowski, K. R. Spinler, J.-W. Shin, M. Tewari, F. Rehfeldt, D. W. Speicher, D. E. Discher, Nuclear lamin-a scales with tissue stiffness and enhances matrix-directed differentiation, Science 341 (6149) (2013) 1240104. doi:10.1126/science.1240104.

[30] E. C. Chittock, S. Latwiel, T. C. R. Miller, C. W. Müller, Molecular architecture of polycomb repressive complexes, Biochem Soc Trans 45 (1) (2017) 193–205. doi:10.1042/BST20160173.

[31] B. van Steensel, A. S. Belmont, Lamina-associated domains: Links with chromosome architecture, heterochromatin, and gene repression, Cell 169 (5) (2017) 780–791. doi:10.1016/j.cell.2017.04.022.

[32] W. Meuleman, D. Peric-Hupkes, J. Kind, J.-B. Beaudry, L. Pagie, M. Kellis, M. Reinders, L. Wessels, B. van Steensel, Constitutive nuclear lamina-genome interactions are highly conserved and associated with a/t-rich sequence, Genome Res 23 (2) (2013) 270–80. doi:10.1101/gr.141028.112.

[33] C. A. M. La Porta, S. Zapperi, Explaining the dynamics of tumor aggressiveness: At the crossroads between biology, artificial intelligence and complex systems, Semin Cancer Biol 53 (2018) 42–47. doi:10.1016/j.semcancer.2018.07.003.

[34] F. Font-Clos, S. Zapperi, C. A. La Porta, Classification of triple-negative breast cancers through a boolean network model of the epithelial-mesenchymal transition, Cell Systems 12 (5) (2021) 457–462.

[35] C. A. M. La Porta, Drug resistance in melanoma: new perspectives, Curr Med Chem 14 (4) (2007) 387–91. doi:10.2174/092986707779941078.

[36] C.-J. Chang, J.-Y. Yang, W. Xia, C.-T. Chen, X. Xie, C.-H. Chao, W. A. Woodward, J.-M. Hsu, G. N. Hortobagyi, M.-C. Hung, Ezh2 promotes expansion of breast tumor initiating cells through activation of raf1-β-catenin signaling, Cancer cell 19 (1) (2011) 86–100.

[37] Y. Wen, J. Cai, Y. Hou, Z. Huang, Z. Wang, Role of ezh2 in cancer stem cells: from biological insight to a therapeutic target, Oncotarget 8 (23) (2017) 37974.

[38] E. Rheinbay, M. L. Suvà, S. M. Gillespie, H. Wakimoto, A. P. Patel, M. Shahid, O. Oksuz, S. D. Rabkin, R. L. Martuza, M. N. Rivera, D. N. Louis, S. Kasif, A. S. Chi, B. E. Bernstein, An aberrant transcription factor network essential for wnt signaling and stem cell maintenance in glioblastoma, Cell Rep 3 (5) (2013) 1567–79. doi:10.1016/j.celrep.2013.04.021.

[39] A. Natsume, M. Ito, K. Katsushima, F. Ohka, A. Hatanaka, K. Shinjo, S. Sato, S. Takahashi, Y. Ishikawa, I. Takeuchi, H. Shimogawa, M. Uesugi, H. Okano, S. U. Kim, T. Wakabayashi, J.-P. J. Issa, Y. Sekido, Y. Kondo, Chromatin regulator prc2 is a key regulator of epigenetic plasticity in glioblastoma, Cancer Res 73 (14) (2013) 4559–70. doi:10.1158/0008-5472.CAN-13-0109.

[40] L. Gan, Y. Yang, Q. Li, Y. Feng, T. Liu, W. Guo, Epigenetic regulation of cancer progression by ezh2: from biological insights to therapeutic potential, Biomark Res 6 (2018) 10. doi:10.1186/s40364-018-0122-2.

[41] H. Yamaguchi, M.-C. Hung, Regulation and role of ezh2 in cancer, Cancer Res Treat 46 (3) (2014) 209–22. doi:10.4143/crt.2014.46.3.209.